

Structural performance monitoring of an urban footbridge

P.S. Xi, X.W. Ye*, T. Jin and B. Chen

Department of Civil Engineering, Zhejiang University, Hangzhou 310058, China

(Received November 20, 2017, Revised February 13, 2018, Accepted February 19, 2018)

Abstract. This paper presents the structural performance monitoring of an urban footbridge located in Hangzhou, China. The structural health monitoring (SHM) system is designed and implemented for the footbridge to monitor the structural responses of the footbridge and to ensure the structural safety during the period of operation. The monitoring data of stress and displacement measured by the fiber Bragg grating (FBG)-based sensors installed at the critical locations are used to analyze and assess the operation performance of the footbridge. A linear regression method is applied to separate the temperature effect from the stress monitoring data measured by the FBG-based strain sensors. In addition, the static vertical displacement of the footbridge measured by the FBG-based hydrostatic level gauges are presented and compared with the dynamic displacement remotely measured by a machine vision-based measurement system. Based on the examination of the monitored stress and displacement data, the structural safety evaluation is executed in combination with the defined condition index.

Keywords: structural health monitoring; urban footbridge; optical fiber sensor; linear regression model; machine vision; safety evaluation

1. Introduction

In the last two decades, many bridge structures have been built for the roadway and railway transportations in China. These bridges play a pivotal role in the transportation systems for the purpose of providing channels over the straits, rivers and valleys. During the operational stage, they are always suffered from a variety of stochastic external loads such as highway traffic, railway traffic, wind loading, and temperature effect. Under the combined action of these external loads, some types of damage such as cracking, corrosion and fatigue will be inevitably occurred on the key structural components of bridges, eventually resulting in the destruction of bridges and civilian casualties. Therefore, the appropriate evaluation of the in-service structural performance and safety condition of a bridge has been a valuable topic concerned by the researchers and engineers all over the world.

Recently, the development of structural health monitoring (SHM) technology for tracing, assessment and supervision of bridge structures has gained significant advances and reached a certain level of maturity (Ko and Ni 2005). The long-term SHM systems have been broadly implemented to dynamically track the structural behaviors (e.g., acceleration, strain and displacement) of instrumented bridges in a continuous and real-time manner (Ni *et al.* 2010, Ye *et*

*Corresponding author, Associate Professor, E-mail: cexwye@zju.edu.cn

al. 2013a, Ye *et al.* 2014, Ye *et al.* 2015, Ye *et al.* 2017, Ye *et al.* 2018a, b). The massive amounts of data measured from an SHM system can be employed to analyze anomalies in external loads and structural responses, identify the possible damage at an early stage to ensure bridge structural safety, and provide the evidences and instructions for planning and optimizing the maintenance and rehabilitation actions.

In general, a typical SHM system is composed of three major parts: the sensor system, the data processing system (data acquisition, transmission and storage), and the structural health evaluation system. Nowadays, the traditional sensors are mostly used in the SHM system and based on the electrical signals which may be affected by electromagnetic interference. Additionally, these sensors are limited to measure only one parameter at each location. Nowadays, several advanced sensing technologies are developed for bridge health monitoring. Amongst them, the optical fiber sensor has been widely used in practice. The bridge health monitoring systems using diversified optical fiber sensors are reported in the literature (Ni *et al.* 2012a, Rodrigues *et al.* 2012, Surre *et al.* 2013, Ye *et al.* 2013b, Ye *et al.* 2016a). Lin *et al.* (2005) developed two novel fiber Bragg grating (FBG) monitoring systems and used them for the real-time measurement of the process of local scour. Mokhtar *et al.* (2012) showed the specially designed and packaged sensor systems for combined strain and temperature measurements and applied this system in a lightweight arch bridge. Furthermore, the measurement of the static vertical displacement of bridges (Yau *et al.* 2013), acceleration response of footbridges (Xu and Wu 2007), and temperature and strain of bridges were also analyzed by use of FBG sensors (Chan *et al.* 2006, Ye *et al.* 2012).

In this paper, an on-line SHM system installed on an urban footbridge located in Hangzhou, China is introduced and the arrangement of the optical fiber sensors is detailed described. The statistical analyses of the monitoring data acquired from the FBG sensors are conducted to supervise the in-service condition of key structural components of the footbridge. Considering the temperature load on the bridge, a linear regression method is applied to separate the temperature effect from the strain monitoring data. The structural displacements of the footbridge measured by the hydrostatic level gauges and machine vision technology are analyzed and presented. The structural safety evaluation is conducted based on the examination of the monitored stress and displacement data with the defined condition index.

2. Structural health monitoring system of the footbridge

2.1 Structural features of the footbridge

The investigated footbridge is located in Hangzhou, China and was opened to operation in 2010. The overall view of the footbridge is shown in Fig. 1. This footbridge has a total length of 45.5 m and a height of 22 m, stretching across two viaducts and an urban road. As shown in Fig. 2, the superstructure of the footbridge is made of groove box girders with a width of 7.6 m and bilateral ribs with a height of 2.4 m. The bridge floor includes handrail, ornament and pavement. Many sensors were installed in the steel box girders for evaluating the structural performance.

2.2 Structural health monitoring system

Aiming to monitor the structural responses and ensure the structural safety during the in-service period, the bridge owner has designed and implemented a continuous long-term SHM system on

the footbridge since 2010. As illustrated in Fig. 3, this system includes four major subsystems: sensors subsystem, data acquisition and transmission subsystem, data processing and control subsystem, and structural health diagnosis and warning subsystem.

The sensor subsystem includes strain sensors, temperature sensors, acceleration sensors, and hydrostatic level gauges. These sensors measured the data of bridge condition by a signal acquisition device which was connected to the data processing computer. The data acquisition and transmission subsystem includes signal acquisition device and corresponding storage device. The automatic signal acquisition procedure was operated in the device to record the signals with different frequencies and generate the database files which were submitted to the data-processing host computer. The signal acquisition and transmission subsystem was continuously operated since the end of 2010, except for accidental interruptions due to some site problems. Amounts of measured data were processed, analyzed and interpreted by the data processing and control subsystem. The dynamic responses and changing physical conditions of the instrumented bridge structure, i.e., strain, displacement, temperature and acceleration, were obtained and used for diagnosing the pre-hazard and post-hazard condition in structural health diagnosis and warning subsystem.



Fig. 1 Photo of the footbridge

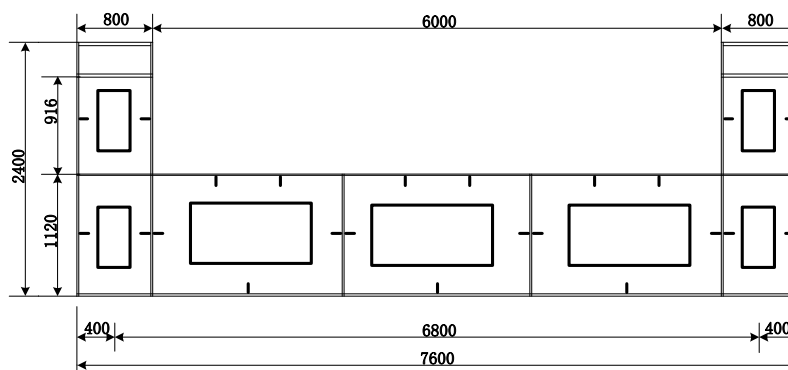


Fig. 2 Cross section of the footbridge (unit: mm)

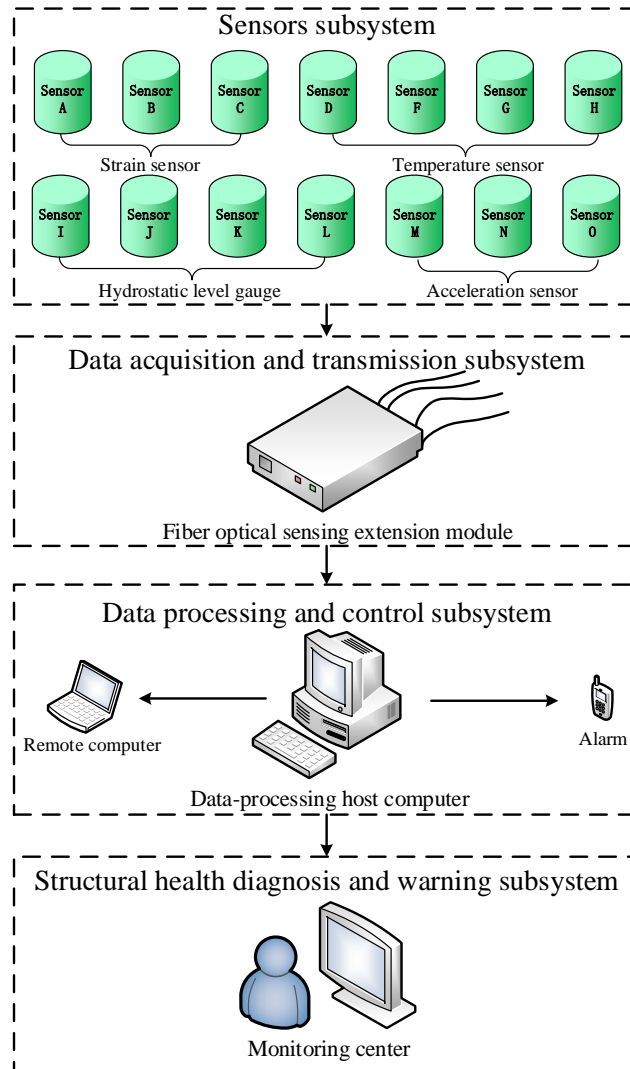
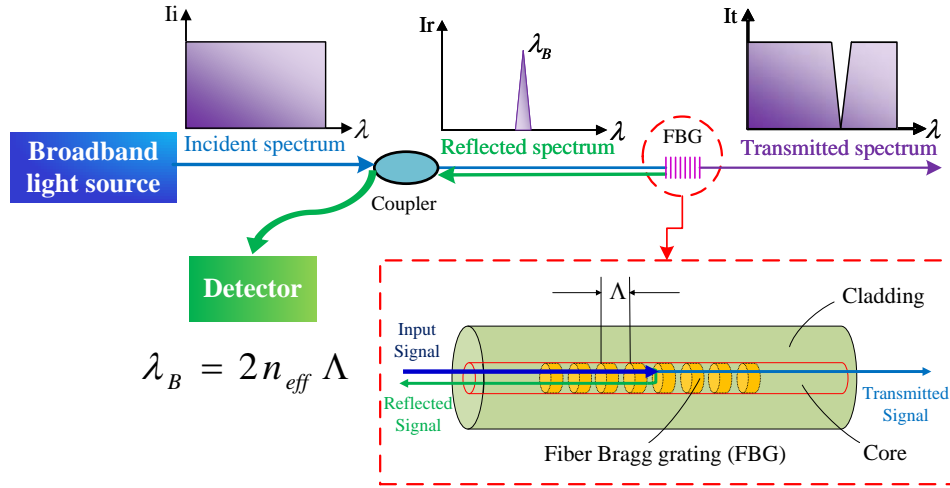


Fig. 3 Architecture of SHM system

2.3 FBG-based monitoring subsystem

An optical fiber sensor is a sensor that uses optical fiber to measure strain, temperature and other quantities. According to the sensing principle, the optical fiber sensors can be segmented into different types. Among these sensors, the FBG sensors have several advantages and thus were selected to apply in the SHM system of the footbridge. One of the advantages of FBG sensors is the immunity of electrical interference, so they can be applied in a hostile environment. In addition, a special advantage reflecting in the transmission performance is that they can be serially placed along in a single optical fiber with little signal loss. For example, a large number of FBG sensors with different wavelength ranges can be applied at multiple points of the whole structure and transmit the data to a distant interrogator through a long length optical fiber.



$$\lambda_B = 2n_{eff} \Lambda$$

Fig. 4 Mechanism of FBG sensor

According to the Bragg's law, when a beam of white broadband light is traveling through the FBG sensor at a particular wavelength, the Bragg wavelength is reflected which is related to the grating period, as illustrated in Fig. 4. The Bragg wavelength, λ_B can be expressed by (Ye *et al.* 2014)

$$\lambda_B = 2n_{eff} \Lambda \tag{1}$$

where λ_B is the center wavelength, n_{eff} is the effective index of refraction, and Λ is the grating period which means the distance between two points of the same refractive index.

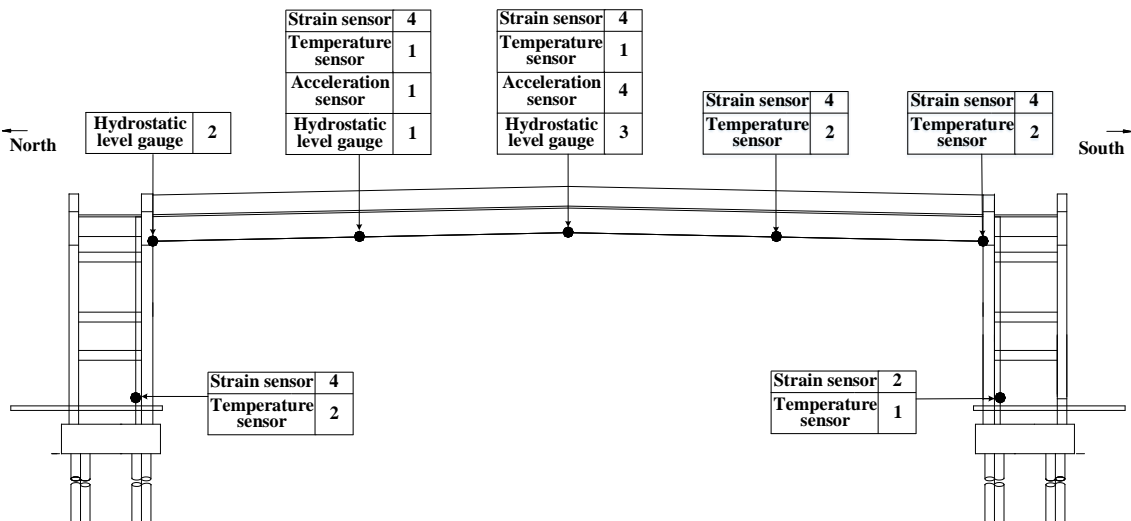


Fig. 5 Deployment of FBG-based sensors

As shown in Fig. 5, for the SHM system of the footbridge, twenty-three measurement points are determined in the footbridge. The FBG-based monitoring subsystem contains four types of sensors: FBG-based strain sensors, FBG-based temperature sensors, FBG-based acceleration sensors, and FBG-based hydrostatic level gauges. The FBG-based strain sensors were deployed at the steel box girders and embedded in the square walls to monitor the stress change of each measurement point. Due to the FBG-based sensors are dual sensitivity to stress and temperature, the FBG-based temperature sensor was installed adjacent to the measurement point of FBG-based strain sensor as the temperature compensation sensor to eliminate the effect of temperature. In addition, the FBG-based acceleration sensors were utilized to monitor the structural dynamic condition, and the FBG-based hydrostatic level gauges were applied to measure the structural displacement of the footbridge deck.

3. Structural stress monitoring of the footbridge

3.1 FBG-based strain and temperature sensor

The FBG-based strain sensor is a device used to measure the strain on an objective structure. The most common type of the FBG-based strain sensor includes the surface mounted FBG-based strain sensor and the embedded FBG-based strain sensor. Temperature and strain cannot be measured separately by only measuring the change of wavelength from one FBG sensor which is sensitive to both influences. Both the change of strain and temperature can cause the shift in the reflected Bragg wavelength through the mechanical force and thermal expansion. One approach to resolve this issue is to use a reference FBG sensor which is only sensitive to the thermal effect. By employing two independent FBG sensors attached to the same point, the wavelength shift caused by the strain can be expressed as

$$\Delta\lambda_{B\varepsilon} = \lambda_{B\varepsilon}\Delta\varepsilon \quad (2)$$

where $\lambda_{B\varepsilon}$ is the photoelastic coefficient of the fiber material, and the shift of wavelength caused by the temperature can be obtained by

$$\Delta\lambda_{BT} = \lambda_{BT}\Delta T \quad (3)$$

where λ_{BT} is the thermal expansion coefficient of the fiber material, and it can be determined by an experiment that the FBG sensor is located in the metal package and exhibited no response to the strain. This way enables the FBG sensor acting as a temperature-only sensor which is immune to the effect of strain. The compensation mechanism of the temperature sensor is utilized to eliminate the temperature effect from the strain sensor by

$$\Delta\lambda_B = \lambda_{B\varepsilon}\Delta\varepsilon + \lambda_{BT}\Delta T \quad (4)$$

3.2 Deployment of FBG-based strain and temperature sensors

As shown in Fig. 6, the monitoring scheme includes the installation of sixteen surface mounted FBG-based strain sensors to measure the strain in the box girder, six embedded FBG-based strain

sensors to measure the strain in the concrete, and nine FBG-based temperature sensors to measure the temperature in the structure. Utilizing the multiplexing ability of the FBG-based sensor, the sensors were linked to an optical fiber network by using the optical fiber cables. The end of each optical fiber link was terminated with a fiber grating demodulation to connect the sensor subsystem to the data acquisition subsystem. Figs. 7 and 8 show the photos of the FBG-based strain sensor and the FBG-based temperature sensor. Table 1 lists the technical parameters of the FBG-based strain sensor. Table 2 lists the technical parameters of the FBG-based temperature sensor.

Table 1 Technical parameters of FBG-based surface mounted strain sensor

Item	Value
Measurement range	$\pm 1500 \mu\epsilon$
Sampling frequency	1 Hz
Resolution ratio	$0.1 \mu\epsilon$
Precision	1‰ F.S.
Wavelength range	1525 nm~1565 nm
Temperature range	$-30^{\circ}\text{C} \sim 120^{\circ}\text{C}$
Sensor size	$\Phi 7 \times 94 \text{ mm}$

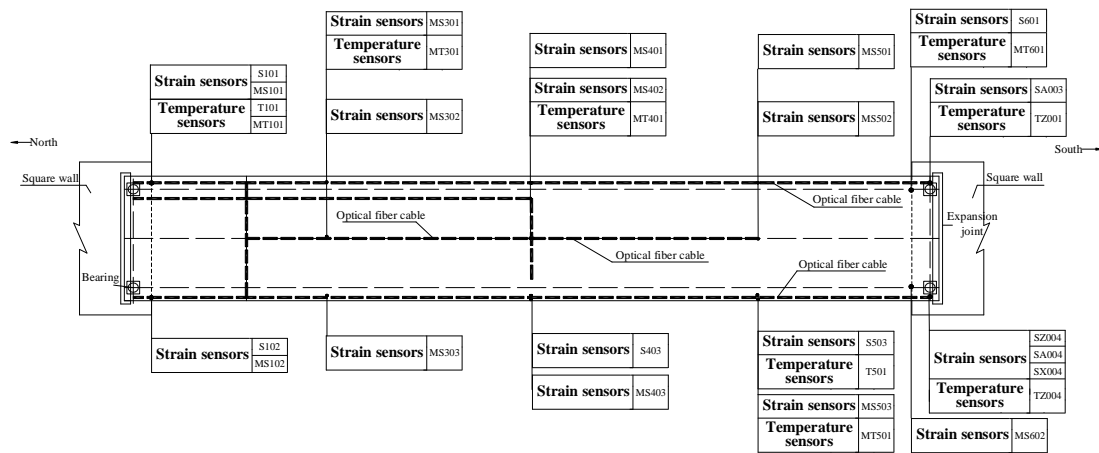


Fig. 6 Deployment of FBG-based strain and temperature sensors



Fig. 7 FBG-based strain sensor

Table 2 Technical parameters of FBG-based temperature sensor

Item	Value
Measurement range	-30 °C~180°C
Sampling frequency	1 Hz
Resolution ratio	0.01 °C
Precision	±0.5 °C
Wavelength range	1525 nm~1565 nm
Temperature range	-30°C~180°C
Sensor size	Φ8×88 mm



Fig. 8 FBG-based temperature sensor

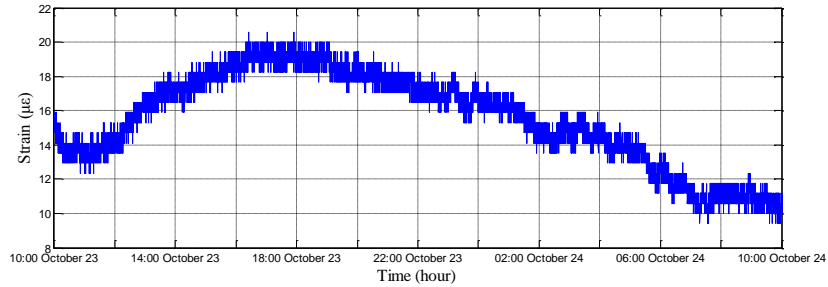
3.3 Analysis of measured strain monitoring data

3.3.1 Strain monitoring data from FBG-based sensors

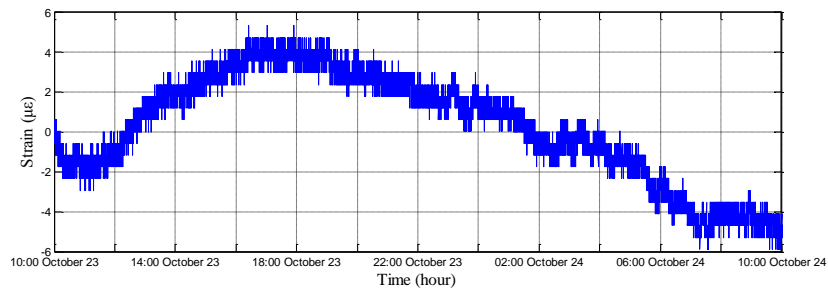
The aim of strain monitoring is to acquire detail information about the structural stress under the operational condition. The structural stress directly indicates the strength safety of the crucial structural component and contributes to the structural condition assessment. In this section, several sets of strain monitoring data from the FBG-based strain sensors installed on the footbridge at three sections, i.e., the northern quarter-span section, the mid-span section, and the southern quarter-span section, are processed and presented.

The temperature and strain measurement data from 23 October 2016 to 24 October 2016 are analyzed to illustrate the strain statement of the footbridge. The strain conditions on the northern quarter-span section are shown in Figs. 9(a), 10(a) and 11(a), and those along the eastern side of the footbridge are shown in Figs. 9(a), 12(a) and 13(a). The strain time histories derived from the measured strain data through compensating the temperature effect. The strain data measured at 10:00 am on 23 October 2016 are taken as the baseline data to observe the relative strain change for one day, as shown in Figs. 9(b), 10(b), 11(b), 12(b) and 13(b).

Figs. 9(a), 10(a), 11(a), 12(a) and 13(a) illustrate the measured daily strain responses. It can be found that the daily strain time histories of the selected points possess a periodic variation characteristic in the shape of the curve and magnitude of amplitude. The measured strain data at the critical points are all within the normal limits by comparing with the designed threshold values as listed in Table 3.

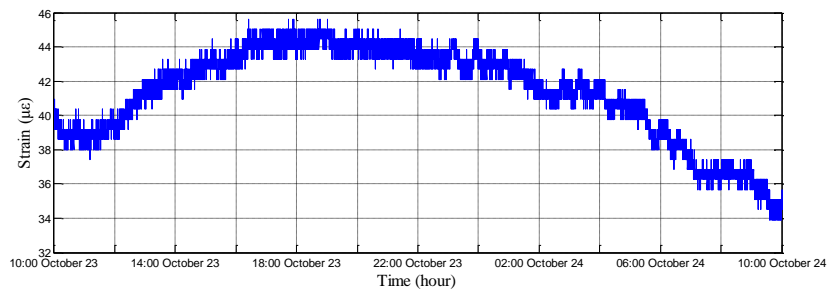


(a) One-day monitoring data of strain response

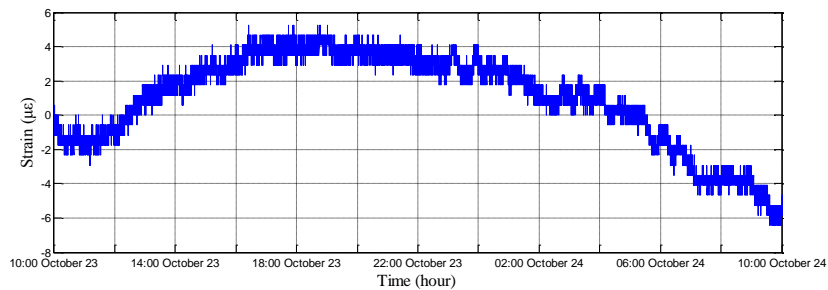


(b) One-day relative strain change

Fig. 9 Strain time history of sensor MS301

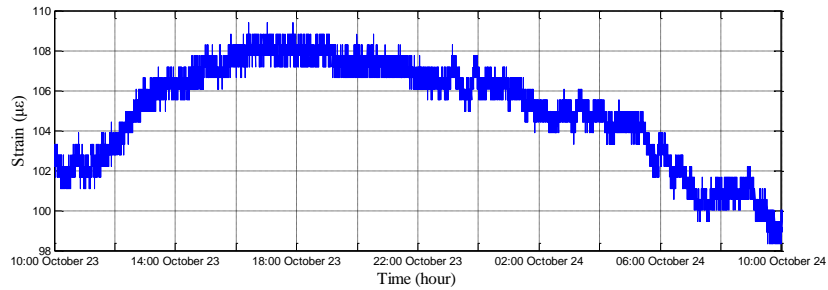


(a) One-day monitoring data of strain response

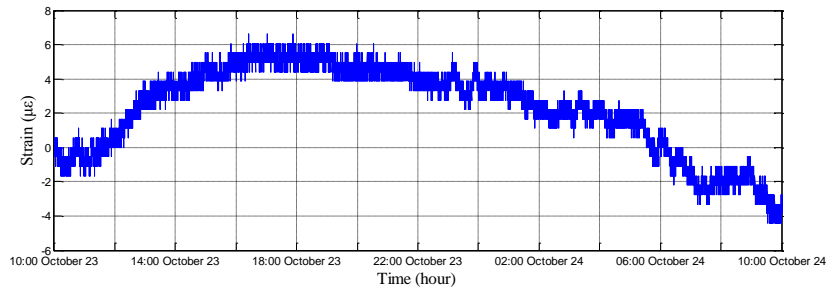


(b) One-day relative strain change

Fig. 10 Strain time history of sensor MS302

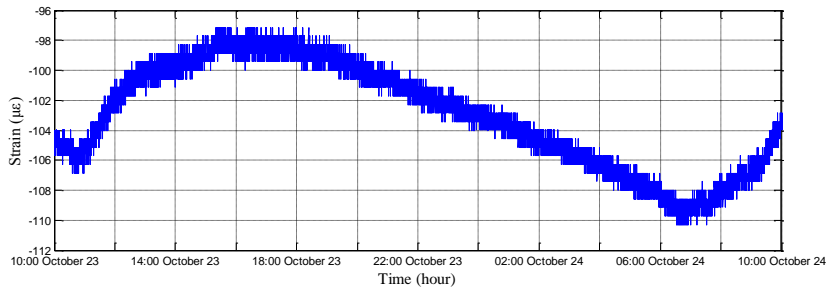


(a) One-day monitoring data of strain response

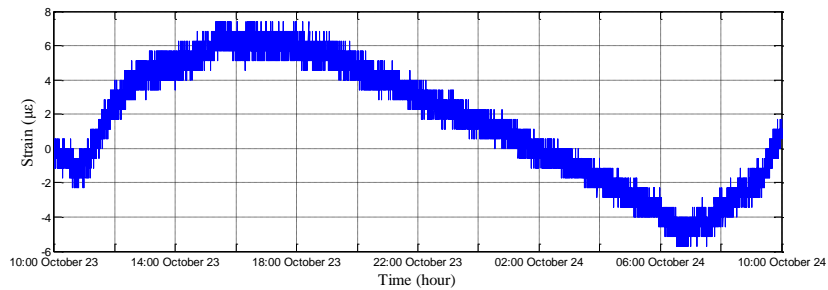


(b) One-day relative strain change

Fig. 11 Strain time history of sensor MS303

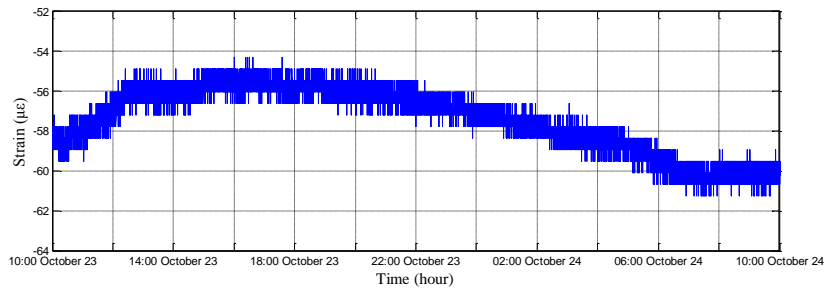


(a) One-day monitoring data of strain response

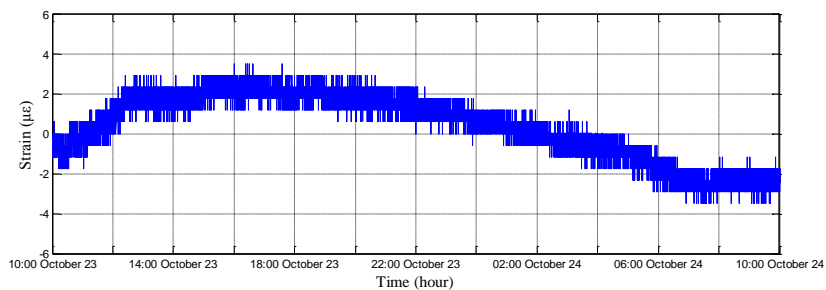


(b) One-day relative strain change

Fig. 12 Strain time history of sensor MS401



(a) One-day monitoring data of strain response



(b) One-day relative strain change

Fig. 13 Strain time history of sensor MS501

Table 3 Designed threshold values of structural strain ($\mu\epsilon$)

Sensor	First-level threshold	Second-level threshold	Compression threshold
MS301	545	216	-182
MS302	545	216	-182
MS303	545	216	-182
MS401	545	216	-182
MS501	545	216	-182

For the one-day relative strain change, as shown in Figs. 9(b), 10(b), 11(b), 12(b) and 13(b), it should be noted that the temperature effect has a significant impact on these three sections of the bridge structure. The strain increases in the morning and reaches the peak at about 4:00 pm, which is attributed to the environmental temperature. As to the northern quarter-span section, the relative strain changes present the same periodic shape of curve and magnitude of amplitude, which means that these three points in the section have similar characteristics under the effect of external load. For the strain response along the eastern side of the bridge, it is easy to obtain from Figs. 9(b), 12(b) and 13(b) that the measured strain data in the mid-span section are obviously higher than those of other two sections.

3.3.2 Separation of temperature effect

The in-service strain monitoring data acquired from the sensors installed on the steel box girder are mainly suffered from the impact of three types of loads, i.e., pedestrian, wind and temperature.

The long-term measurement strain data are resulted from a combination of these loading effects and include different strain components. By observing the periodic shape of the strain time history, it is obvious that there are trend ingredients (low-frequency components) in all the strain time histories which can be considered to be the daily cycle effect of temperature variation (Ni *et al.* 2012b).

As reflected from the strain monitoring data, the box girder is mainly behaved as expansion and constriction along the longitudinal direction during the operation period under the temperature effect. It also will undergo flexural bending under the impact of pedestrian loads. These two types of different strain responses are mixed in the strain monitoring data. Thus, it is essential to characterize them separately when each effect on the structural behavior is required to be quantified. In this section, a linear regression method is proposed to decompose the measured strain data by use of a linear regression equation with sinusoidal components.

The general equation is selected based on the linear regression equation with sinusoidal components to fit the fluctuant characteristic of the strain data. The model is defined as

$$\sigma(t) = a_1 + a_2 t + a_3 t \sin(a_4 t) \quad (5)$$

where $\sigma(t)$ is the strain data, a_1 and a_2 are the regression coefficients of the linear regression model which represent the intercept and slope, a_3 is the amplitude of the sine wave, and a_4 is the frequency parameter.

Many methods have been developed for parameter estimation and inference in a linear regression model. The least-squares estimation method is chosen in this study to estimate the parameters. Assuming that a simple data set includes n data pairs, such as the independent variable t_i ($i=1, \dots, n$) and the corresponding dependent variable σ_i ($i=1, \dots, n$), the least-squares estimation method finds the optimum parameter values of the selected regression model when the sum of the square residuals (SSR) reaches the minimum value, and SSR is given by

$$SSR = \sum_{i=1}^n (\sigma_i - \sigma(t_i))^2 \quad (6)$$

where n is the total number of the selected data, σ_i is the i_{th} value of the strain variable to be predicted, and $\sigma(t_i)$ is the predicted value of σ_i .

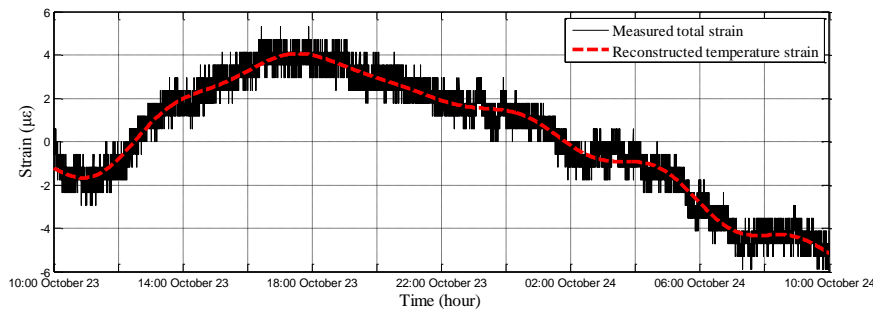


Fig. 14 Decomposed strain data of sensor MS301

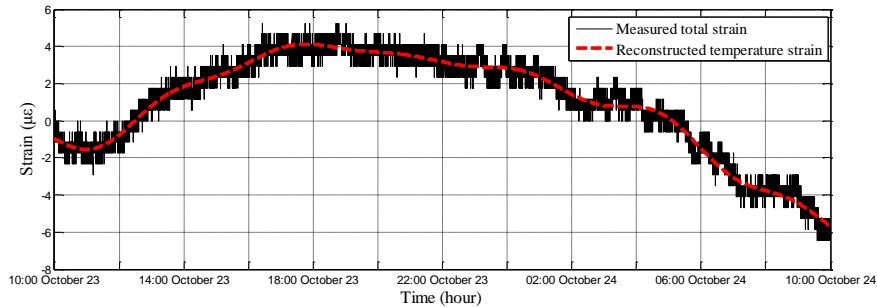


Fig. 15 Decomposed strain data of sensor MS302

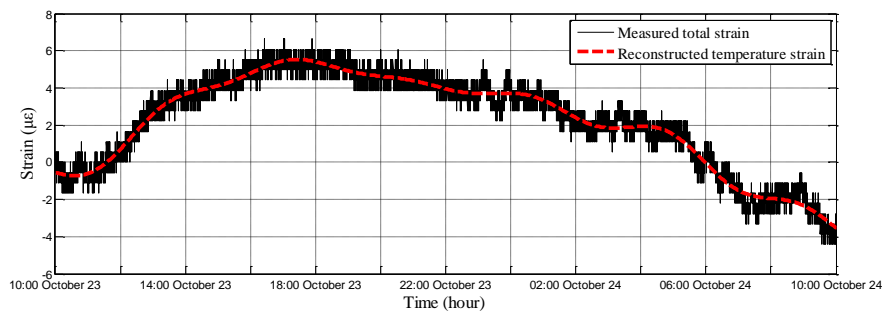


Fig. 16 Decomposed strain data of sensor MS303

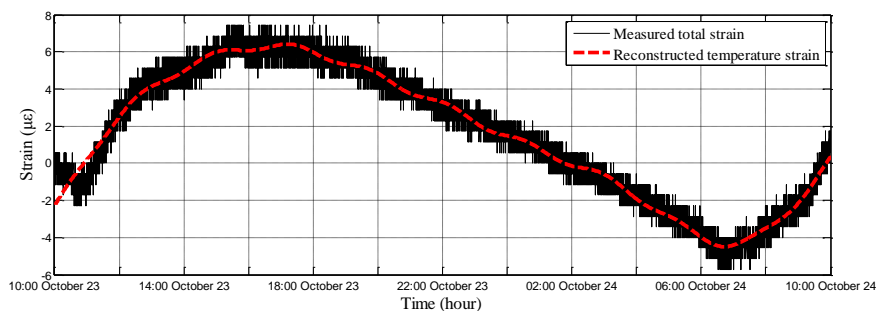


Fig. 17 Decomposed strain data of sensor MS401

Then, the measured strain signals are decomposed into high-frequency and low-frequency components. As shown in Figs. 14 to 18, for each measurement point, the high-frequency component is separated and the remaining part (temperature-induced strain) is reconstructed. It is obvious that the low-frequency components can be regarded as the cycle effect of temperature variation. The reconstructed temperature-induced strain time curve has a similar shape and magnitude with the initial strain time history.

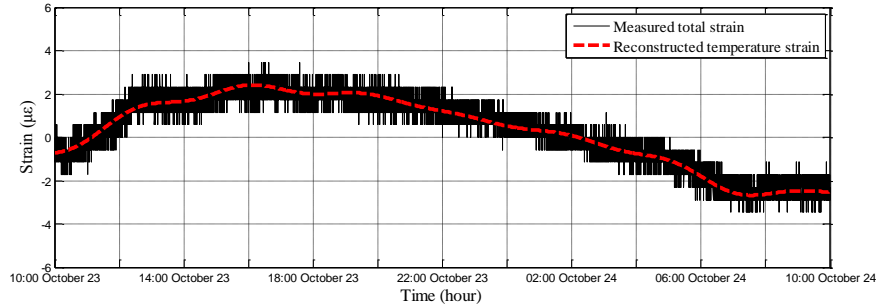


Fig. 18 Decomposed strain data of sensor MS501

4. Structural displacement monitoring of the footbridge

4.1 FBG-based hydrostatic level gauge

Structural displacement measurement is of significance in assessing the structural condition and safety (Marecos 1978). In the SHM system of the investigated footbridge, the hydrostatic level measurement system is applied to monitor the structural displacement of the bridge deck. The FBG-based hydrostatic level gauges measure the hydrostatic level positions along the structure which is realized by a circuit filled with proper liquid that connects the FBG-based hydrostatic level gauges fixed on the structure. For each FBG-based hydrostatic level gauge, the structural physical property is transformed into the optical signal. The schematic diagram of the FBG-based hydrostatic level measurement system is shown in Fig. 19. The FBG-based hydrostatic level gauges are installed at the selected sections of the bridge deck and connected with each other to form a liquid circuit. The variation of the free liquid level inside the metal container is recorded which is caused by the structural deformation from its initial position. Inside the container, a suspended floater partially immerses in the liquid and connects a load cell which is used to measure the immersed weight through the FBG sensor.

According to the Archimedes' principle, the height of the internal liquid can be obtained by the magnitude of the immersed weight of the floater, which is

$$h = \frac{B}{\rho g A} = \frac{mg - W}{\rho g A} \quad (7)$$

where B is the buoyancy force which can be obtained by subtracting the apparent weight W from the true weight mg , h is the immersion depth of the floater, and ρ is the density of the liquid. The change of the corresponding liquid level can be calculated by measuring the apparently immersed weight of the floater.

To measure the immersed weight, two FBG-based strain sensors with different wavelengths are installed at the surface of the load cell. The force is transformed into the measurable optical signal. Through eliminating the thermal effect by one FBG sensor, the measured signal due to the change of the relative vertical level of liquid can be derived.

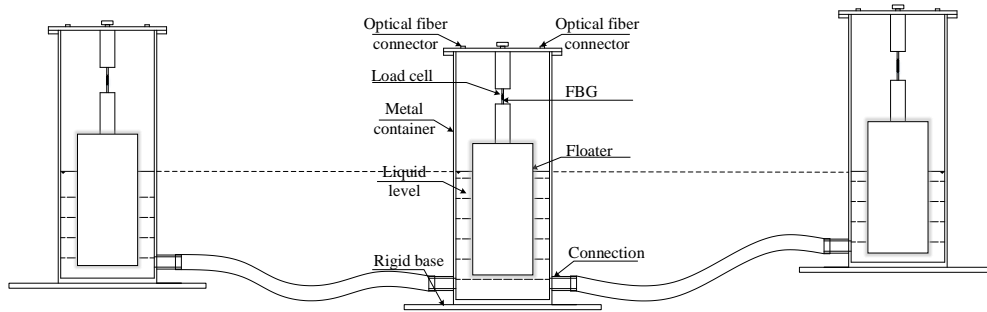
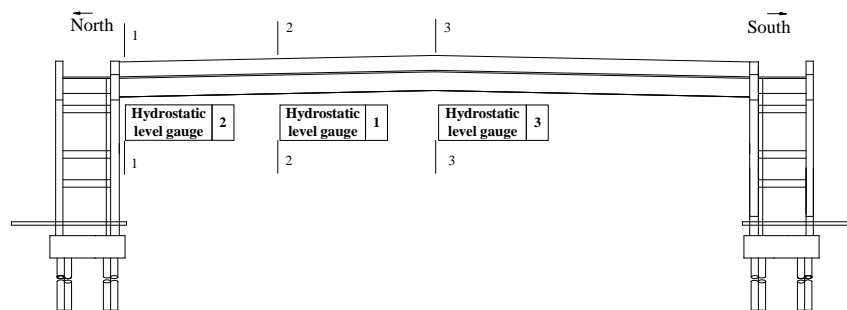


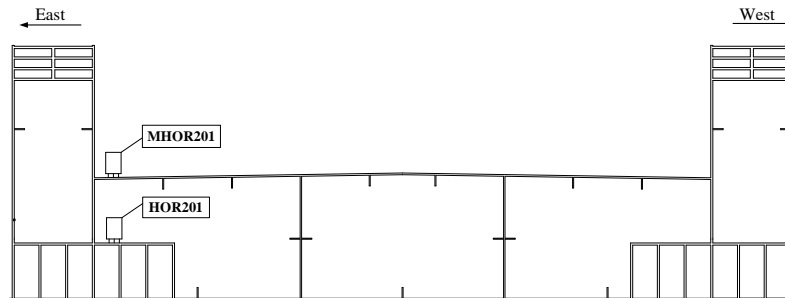
Fig. 19 Schematic diagram of FBG-based hydrostatic level measurement system

4.2 Deployment of FBG-based hydrostatic level gauges

As illustrated in Fig. 20(a), the FBG-based hydrostatic level gauges are deployed at three sections of the bridge deck to measure the structural displacement, which includes the northern support section, quarter-span section, and mid-span section of the bridge as shown in Figs. 20(b) -20(d) respectively. A total of six FBG-based hydrostatic level gauges are installed inside the box girder, and the FBG-based hydrostatic level gauge located at the northern support section serves as the reference point. Fig. 21 shows the FBG-based hydrostatic level gauge. Table 4 lists the technical parameters of the FBG-based hydrostatic level gauge.



(a) Overall layout



(b) Section 1-1

Continued-

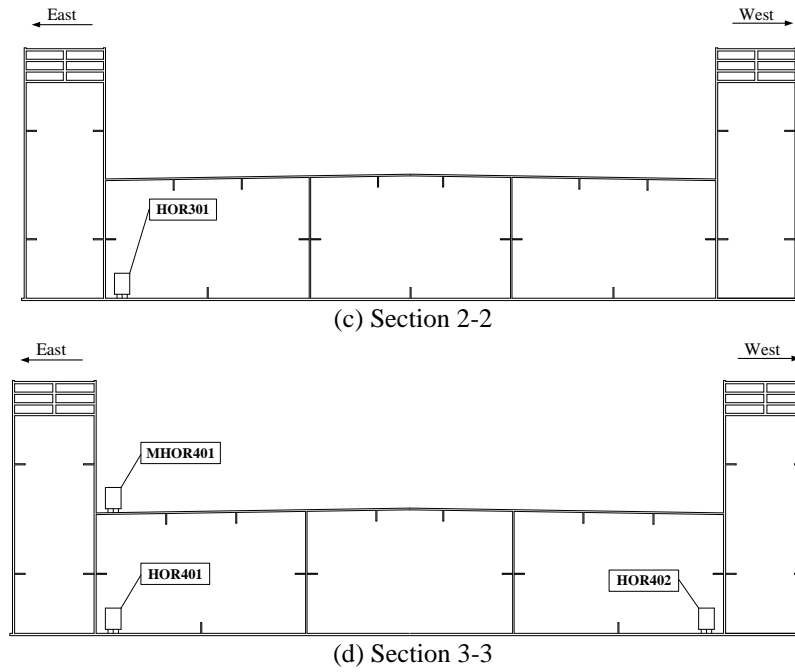


Fig. 20 Deployment of FBG-based hydrostatic level gauges



Fig. 21 FBG-based hydrostatic level gauge

Table 4 Technical parameters of FBG-based hydrostatic level gauge

Item	Value
Measurement range	0-100 mm
Sampling frequency	1 Hz
Resolution ratio	0.01 mm
Precision	1‰ F.S.
Wavelength range	1525 nm~1565 nm
Temperature range	-30℃~85℃
Sensor size	Φ90×200 mm

4.3 Analysis of measured displacement monitoring data

4.3.1 Displacement monitoring data from FBG-based hydrostatic level gauge

In order to assess the displacement condition and structural alignment of the bridge, the displacement monitoring data of three critical sections along the eastern side of the bridge deck, i.e., HOR201, HOR301 and HOR401, are presented and analyzed. The measured displacement data of three measurement points from 23 October 2016 to 24 October 2016 are chosen for analysis. The displacement data measured from the sensors when the installation completes are used to serve as the baseline data. After eliminating the effect of temperature on the measured data, the results of displacement condition of the bridge deck are shown in Figs. 22 to 24.

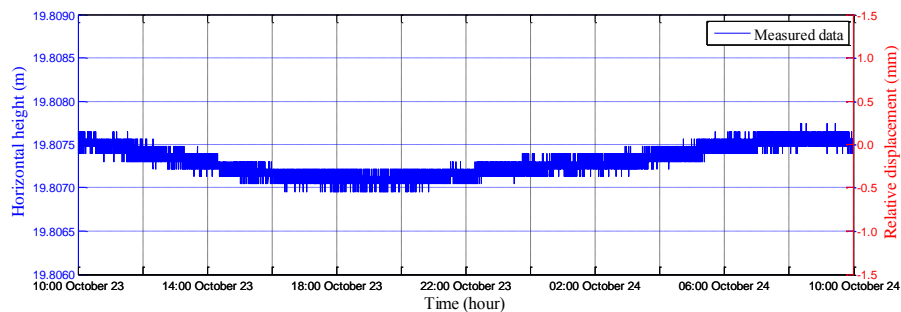


Fig. 22 Displacement time curve at support section (HOR201)

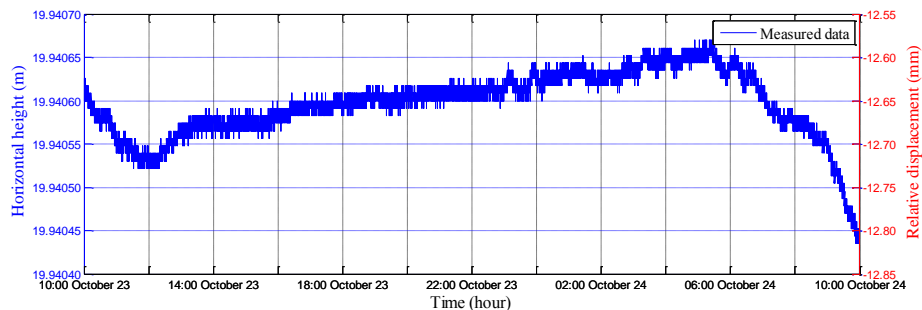


Fig. 23 Displacement time curve at quarter-span section (HOR301)

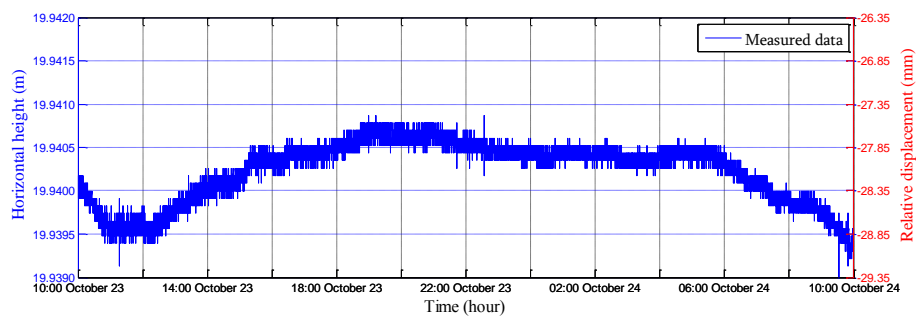


Fig. 24 Displacement time curve at mid-span section (HOR401)

Table 5 Threshold values of measurement points (mm)

Sensor	First-level threshold	Second-level threshold	Upward threshold
HOR201	75.8	16.16	-7.58
HOR301	75.8	16.16	-7.58
HOR401	75.8	16.16	-7.58

As shown in Fig. 22, the structural displacement exhibits a steady trend and the relative displacement is varied between -0.5 mm and 0.5 mm, demonstrating that the supporting structure of the bridge deck is barely affected by the environmental temperature. Figs. 23 and 24 show the displacement condition of the quarter-span and mid-span sections of the bridge deck. It can be observed that there is an obvious variation which may be induced by the daily effect of the differential variation of the temperature experienced by the bridge steel box girder. The maximum relative displacement happens at the mid span-section of the bridge and the vertical displacement at the mid-span section is approximately twice of that at the quarter-span section.

As shown in Table 5, the structural displacement subsystem sets three threshold values as the alarming limits for structural safety assessment. The average accumulated structural displacement at the quarter-span section reaches 11.85 mm within the second-level threshold value. The average accumulated displacement at the mid-span section slightly exceeds the second-level threshold value and reaches 28.35 mm. The maximal value of the structural displacement is much lower than the first-level threshold value.

4.3.2 Dynamic displacement monitoring based on machine vision technology

A machine vision-based displacement measurement system is composed of target objects, a digital camera, a laptop computer, and software (Ye *et al.* 2016b). As shown in the Fig. 25, the high-precision industrial camera was placed at the position approximately 150 m away from the mid-span of the bridge deck. Three high-intensity flashlights as the measurement targets were installed at three sections of the bridge deck, i.e., 1/2 span section, 3/8 span section, and 1/4 span section. The camera is relatively far from the bridge deck, and a 12X-zoom lens is incorporated with the camera to improve the precision and resolution of images. Image data measured by the camera are transferred to the computer through the Ethernet cable for further process of the structural displacement.

As shown in the Fig. 26, a software program is developed to track the motion of each measurement point on the bridge deck. In order to calibrate the actual movement of the flashlight target, a reference point was installed near the second target and a known distance between these two flashlights targets is input into the computer at the beginning of each measurement case. After finishing the above-mentioned procedures, the structural displacement of three selected measurement points on the bridge deck can be measured simultaneously.

Fig. 27 shows the structural displacements of three target points on the footbridge measured by the machine vision-based measurement system at a sampling frequency of 60 Hz. It is seen from Fig. 27 that the structural displacements of the 1/2 span of the bridge deck are slightly larger than those of other two measurement points and are ranged from -2 mm to 2 mm. The similar shape of displacement time curve of three target points indicates that three sections of the bridge deck have homologous dynamic responses under the external load, and the machine vision-based system shows the ability to simultaneously monitor the dynamic responses of three measurement points.

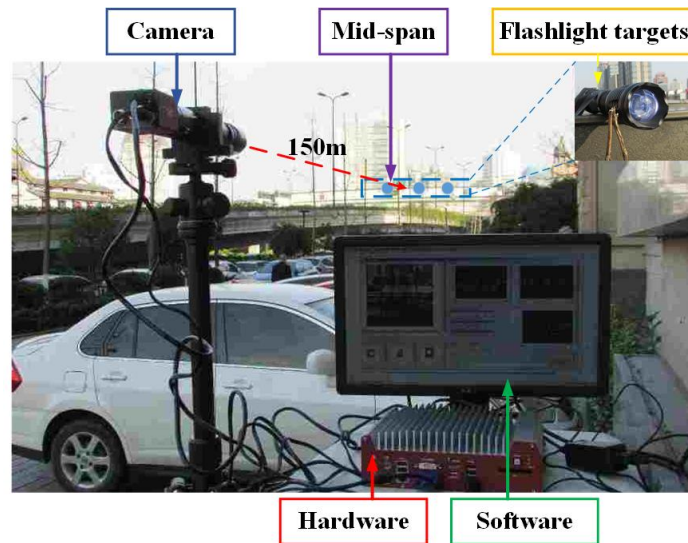


Fig. 25 Experimental setup of vision-based displacement measurement system

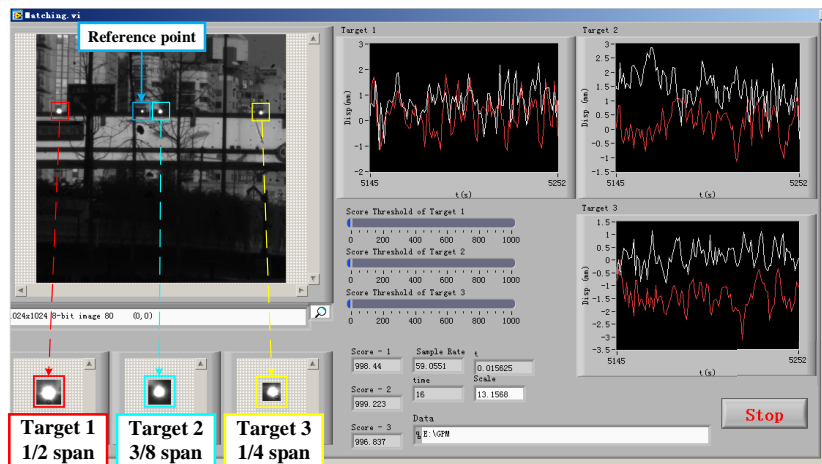


Fig. 26 Software interface of vision-based displacement measurement system

In comparison with the displacement data measured by the FBG-based hydrostatic level gauges, the displacement data measured by the machine vision technology can obtain the structural vibration characteristics of the bridge deck based on the high sampling frequency. In addition, the amplitude of the measured displacement keeps approximately 1 mm which conforms to the static displacement data. Also, there are some relatively large displacements which reach around 2 mm which mainly attribute to a relatively large pedestrian load or wind load.

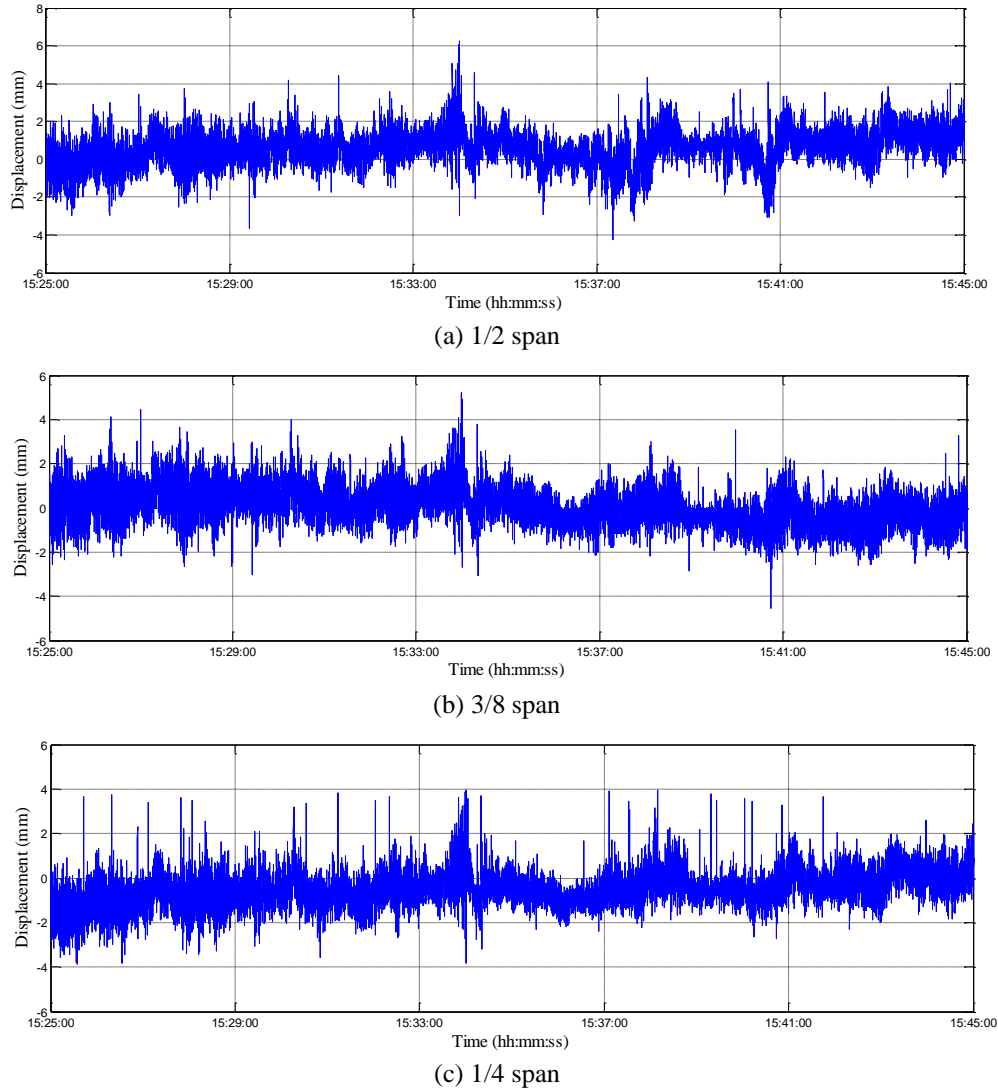


Fig. 27 Measured displacement data of the footbridge

5. Conclusions

In this paper, the long-term SHM system installed on a footbridge was introduced. The stress data measured by the FBG-based strain sensors were analyzed and the temperature effect was separated by a linear regression method. In addition, the structural displacements of the bridge deck measured by the FBG-based hydrostatic level gauges and machine vision technology were comparatively analyzed. The measured stress and displacement data were used to assess the structural safety condition of the bridge during the operation period. The analysis results demonstrate that: (i) the SHM system of the footbridge shows strong stability and reliability in data acquisition and can provide abundant monitoring data of structural responses; (ii) the daily

strain-time curves possess a periodic variation characteristic in the shape of the curve and magnitude of amplitude; (iii) the linear regression model with a sinusoidal component can effectively reconstruct temperature-induced strain from the measured strain data and the least-squares estimation algorithm can estimate the model parameters; (iv) the vertical displacement time curves of the quarter-span section and the mid-span section show an obvious peak and valley which may be suffered from the temperature effect; and (v) the machine vision-based dynamic displacement measurement system can effectively measure the displacement of a bridge with high frequency and accuracy.

Acknowledgments

The work described in this paper was jointly supported by the National Science Foundation of China (Grant No. 51778574), the Fundamental Research Funds for the Central Universities of China (Grant No. 2017QNA4024), and the Key Lab of Structures Dynamic Behavior and Control (Harbin Institute of Technology), Ministry of Education of the PRC.

References

- Chan, T.H., Yu, L., Tam, H.Y., Ni, Y.Q., Liu, S.Y., Chung, W.H. and Cheng, L.K. (2006), "Fiber Bragg grating sensors for structural health monitoring of Tsing Ma bridge: Background and experimental observation", *Eng. Struct.*, **28**(5), 648-659.
- Ko, J.M. and Ni, Y.Q. (2005), "Technology developments in structural health monitoring of large-scale bridges", *Eng. Struct.*, **27**(12), 1715-1725.
- Lin, Y.B., Chen, J.C., Chang, K.C., Chern, J.C. and Lai, J.S. (2005), "Real-time monitoring of local scour by using fiber Bragg grating sensors", *Smart Mater. Struct.*, **14**(4), 664-670.
- Marecos, J. (1978), "The measurement of vertical displacements through water levelling method", *Mater. Struct.*, **11**(5), 361-370.
- Mokhtar, M.R., Owens, K., Kwasny, J., Taylor, S.E., Basheer, P.A.M., Cleland, D., Bai, Y., Sonebi, M., Davis, G., Gupta, A., Hogg, I., Bell, B., Doherty, W., McKeague, S., Moore, D., Greeves, K., Sun, T. and Grattan, K.T.V. (2012), "Fiber-optic strain sensor system with temperature compensation for arch bridge condition monitoring", *IEEE Sens. J.*, **12**(5), 1470-1476.
- Ni, Y.Q., Xia, H.W., Wong, K.Y. and Ko, J.M. (2012b), "In-service condition assessment of bridge deck using long-term monitoring data of strain response", *J. Bridge Eng.*, **17**(6), 876-885.
- Ni, Y.Q., Ye, X.W. and Ko, J.M. (2010), "Monitoring-based fatigue reliability assessment of steel bridges: analytical model and application", *J. Struct. Eng. - ASCE*, **136**(12), 1563-1573.
- Ni, Y.Q., Ye, X.W. and Ko, J.M. (2012a), "Modeling of stress spectrum using long-term monitoring data and finite mixture distributions", *J. Eng. Mech. - ASCE*, **138**(2), 175-183.
- Rodrigues, C., Cavadas, F., Felix, C. and Figueiras, J. (2012), "FBG based strain monitoring in the rehabilitation of a centenary metallic bridge", *Eng. Struct.*, **44**, 281-290.
- Surre, F., Sun, T. and Grattan, K.T. (2013), "Fiber optic strain monitoring for long-term evaluation of a concrete footbridge under extended test conditions", *IEEE Sens. J.*, **13**(3), 1036-1043.
- Xu, Z. D., and Wu, Z. (2007), "Energy damage detection strategy based on acceleration responses for long-span bridge structures", *Eng. Struct.*, **29**(4), 609-617.
- Yau, M.H., Chan, T.H.T., Thambiratnam, D. and Tam, H.Y. (2013), "Static vertical displacement measurement of bridges using fiber Bragg grating (FBG) sensors", *Adv. Struct. Eng.*, **16**(1), 165-176.
- Ye, X.W., Dong, C.Z. and Liu, T. (2016b), "Image-based structural dynamic displacement measurement using different multi-object tracking algorithms", *Smart Struct. Syst.*, **17**(6), 935-956.

- Ye, X.W., Ni, Y.Q. and Yin, J.H. (2013b), "Safety monitoring of railway tunnel construction using FBG sensing technology", *Adv. Struct. Eng.*, **16**(8), 1401-1409.
- Ye, X.W., Ni, Y.Q., Wai, T.T., Wong, K.Y., Zhang, X.M. and Xu, F. (2013a), "A vision-based system for dynamic displacement measurement of long-span bridges: algorithm and verification", *Smart Struct. Syst.*, **12**(3-4), 363-379.
- Ye, X.W., Ni, Y.Q., Wong, K.Y. and Ko, J.M. (2012), "Statistical analysis of stress spectra for fatigue life assessment of steel bridges with structural health monitoring data", *Eng. Struct.*, **45**, 166-176.
- Ye, X.W., Su, Y.H. and Han, J.P. (2014), "Structural health monitoring of civil infrastructure using optical fiber sensing technology: a comprehensive review", *The Scientific World J.*, **2014**, 1-11.
- Ye, X.W., Su, Y.H. and Xi, P.S. (2018b), "Statistical analysis of stress signals from bridge monitoring by FBG system", *Sensors*, **18**(2), 1-14.
- Ye, X.W., Su, Y.H., Xi, P.S., Chen, B. and Han, J.P. (2016a), "Statistical analysis and probabilistic modeling of WIM monitoring data of an instrumented arch bridge", *Smart Struct. Syst.*, **17**(6), 1087-1105.
- Ye, X.W., Xi, P.S., Su, Y.H., Chen, B. and Han, J.P. (2018a), "Stochastic characterization of wind field characteristics of an arch bridge instrumented with structural health monitoring system", *Struct. Saf.*, **71**, 47-56.
- Ye, X.W., Yi, T.H., Dong, C.Z., Liu, T. and Bai, H. (2015), "Multi-point displacement monitoring of bridges using a vision-based approach", *Wind Struct.*, **20**(2), 315-326.
- Ye, X.W., Yi, T.H., Su, Y.H., Liu, T. and Chen, B. (2017), "Strain-based structural condition assessment of an instrumented arch bridge using FBG monitoring data", *Smart Struct. Syst.*, **20**(2), 139-150.